

**Fe-Induced Crystalline-Amorphous Interface Engineering of NiMo-Based Heterostructure  
for Enhanced Water Oxidation**

Junming Zhang<sup>\*,1</sup>, Yingjian Fang<sup>1</sup>, Yao Chen<sup>1</sup>, Yang Gao, Xiaojie Zhang, Tao Tang, Baoqiang Tian,  
He Xiao, Man Zhao, Ergui Luo<sup>\*</sup>, Tianjun Hu, Jianfeng Jia<sup>\*</sup> and Haishun Wu

Key Laboratory of Magnetic Molecules and Magnetic Information Materials of Ministry of  
Education, School of Chemistry and Materials Science, Shanxi Normal University, Taiyuan  
030032, China

---

\* Corresponding authors.

E-mail addresses: zhangjunming@sxnu.edu.cn (J Zhang), luogui1991@sxnu.edu.cn (E. Luo), jiajf@dns.sxnu.edu.cn (J. Jia).

<sup>1</sup> These authors contributed equally to the work.

## Experimental Section

**Materials.** Nickel (II) acetate tetrahydrate  $[\text{Ni}(\text{CH}_3\text{COO})_2 \cdot 4\text{H}_2\text{O}]$ , ammonium molybdate tetrahydrate  $[(\text{NH}_4)_6\text{Mo}_7\text{O}_{24} \cdot 4\text{H}_2\text{O}]$ , iron (III) chloride anhydrous ( $\text{FeCl}_3$ ), ammonium fluoride ( $\text{NH}_4\text{F}$ ), urea  $[\text{CO}(\text{NH}_2)_2]$ , and absolute ethanol ( $\text{C}_2\text{H}_5\text{OH}$ , 95%) were purchased from Sinopharm Chemical Reagent Co. Ltd. (Shanghai, China). All chemicals are of analytical grade and used as received without any further purification. Nickel foam was obtained from Aladdin Co. Ltd. (Shanghai, China). A 5 wt% Nafion solution was purchased from Sigma-Aldrich. All solutions were prepared using Millipore water ( $18.2 \text{ M}\Omega \text{ cm}$ ).

**Material characterizations.** The crystal phase of catalyst was characterized by an X-ray diffractometer (XRD, Rigaku Ultima IV-185) with a  $\text{Cu K}\alpha$  radiation source ( $\lambda = 0.154056 \text{ nm}$ ) in the  $2\theta$  angle range of  $10\text{-}90^\circ$ . The morphologies of samples were analyzed by scanning electron microscope (SEM, JSM-7001F) and transmission electron microscope (TEM, JEM-2100, 200 kV). High-resolution TEM (HRTEM) images and energy dispersive X-ray spectra (EDS) also were obtained on the TEM and SEM, respectively. X-ray photoelectron spectra (XPS) measurements were carried out using a PHI Quantum 2000 with an  $\text{Al K}\alpha$  monochromatic X-ray source operating at 15 kV.

**Electrochemical measurements.** All electrochemical tests were performed on a CHI 660E electrochemical workstation. Electrochemical performance was measured in 1.0 M KOH solution by a conventional three-electrode system, in which the self-supported sample, graphite rod, and  $\text{Hg}/\text{HgO}$  electrode were served as working electrode, counter electrode, and reference electrode, respectively. For comparison, 5 mg of commercial Pt/C or 25 mg of  $\text{RuO}_2$  catalyst was ultrasonically dispersed in a mixed solution containing 0.95 mL of ethanol and millipore water, as well as 0.05 mL of Nafion, and finally dropped on NF ( $1.0 \times 1.0 \text{ cm}^2$ ). All potentials were relative to the reversible hydrogen electrode (RHE) according to the equation of  $E_{\text{RHE}} = E_{\text{Hg}/\text{HgO}} + 0.098 \text{ V} + 0.059\text{pH}$ .

Linear sweep voltammetry (LSV) curves were obtained in  $\text{O}_2$ -saturated KOH solution at a scan rate of  $5 \text{ mV s}^{-1}$  and corrected by 85%  $iR$  compensation. Tafel plots were derived from LSV curves by the equation of  $\eta = a + b \log|j|$ , where 'a' is the Tafel constant, and 'b' is Tafel slope. The electrochemical active surface area (ECSA) was calculated from the double-layer capacitance ( $C_{\text{dl}}$ ) by the equation of  $\text{ECSA} = A \times C_{\text{dl}}/C_s$ , where 'A' is the geometric area, and  $C_s = 40 \mu\text{F cm}^{-2}$ . The

$C_{dl}$  values were obtained from cyclic voltammetry (CV) curves at various scan rates (40, 60, 80, 100, 120  $\text{mV s}^{-1}$ ) within the potential window of 1.024 V-1.124 V. Electrochemical impedance spectroscopy (EIS) was carried out in the frequency range from 100 kHz to 0.1 Hz. The long-term stability of the NiMo(Fe)-20 catalyst was tested in 1.0 M KOH (25 °C) by two methods, namely chronopotentiometry (50  $\text{mA cm}^{-2}$ , 10 h), and accelerated degradation test (ADT, 50  $\text{mV s}^{-1}$ , 2000 cycles).

The turnover frequency (TOF) was calculated by the following equation:  $\text{TOF} = A \times j/4FM$ , where 'j' is the current density, 4 is the number of electron transfer,  $F = 96485 \text{ C mol}^{-1}$ , and M is the number of active site. And M can be calculated by the following equation:  $\text{slope} = n^2F^2M/4RT$ . Moreover, the slope value is obtained from the linear relationship between the oxidation peak current and the scan rate. The electrochemical activation energy ( $E_a$ ) can be obtained by the Arrhenius formula,  $\log j = \text{const} - E_a/RT \ln 10$ , where 'j' is current density at appointed overpotential,  $R = 8.314 \text{ J mol}^{-1} \text{ K}^{-1}$ , 'T' is Kelvin temperature. On the basis of Arrhenius formula, the  $E_a$  can be calculated by the slope of  $\log j$  and  $1/T$  linear curve. The electrochemical water splitting performance was tested with a two-electrode system, the cathode was composed of NF-supported commercial Pt/C catalyst, and the anode was made by NF-loaded commercial  $\text{RuO}_2$  or NiMo-based catalysts.

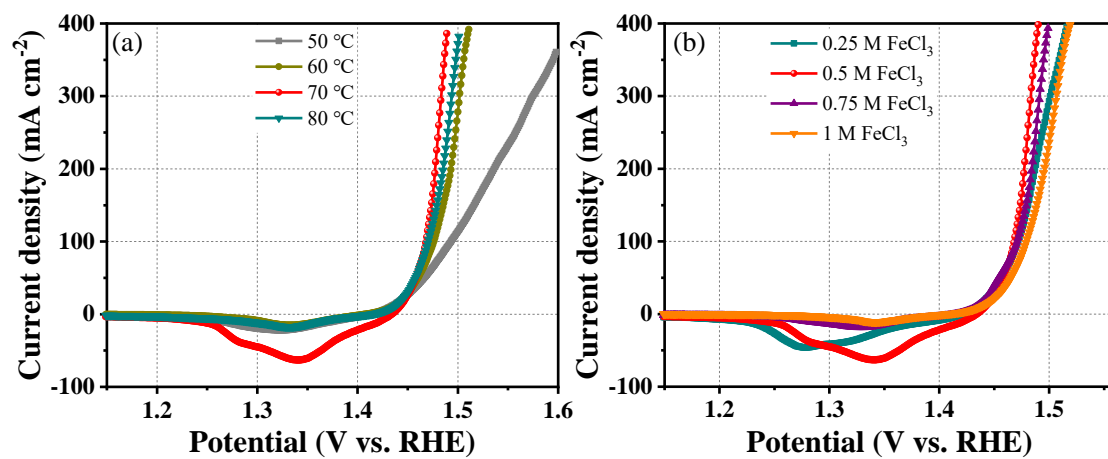


Figure S1. Screening the synthesis conditions (reaction time and concentration of FeCl<sub>3</sub> solution) of the NiMo(Fe)-20 catalyst.

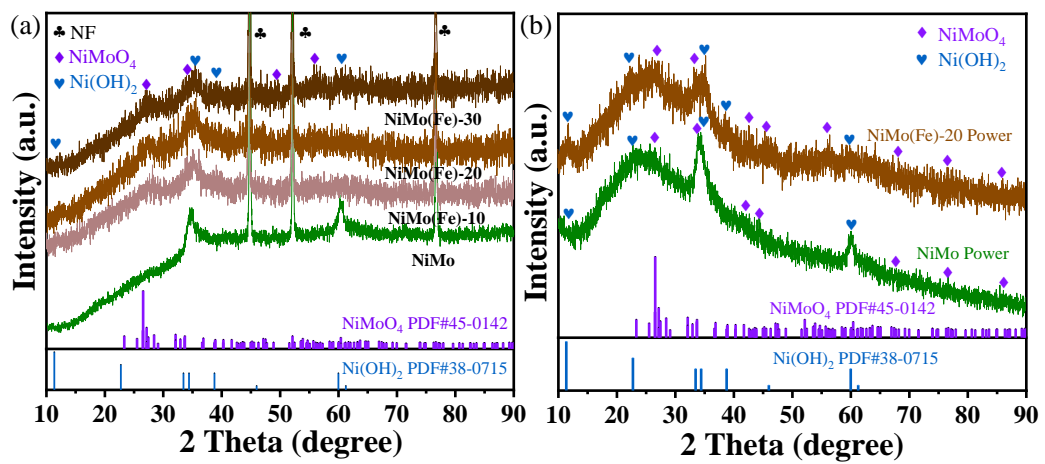


Figure S2. XRD patterns of self-supported four NiMo-based samples (a), and two NiMo-based power (b).

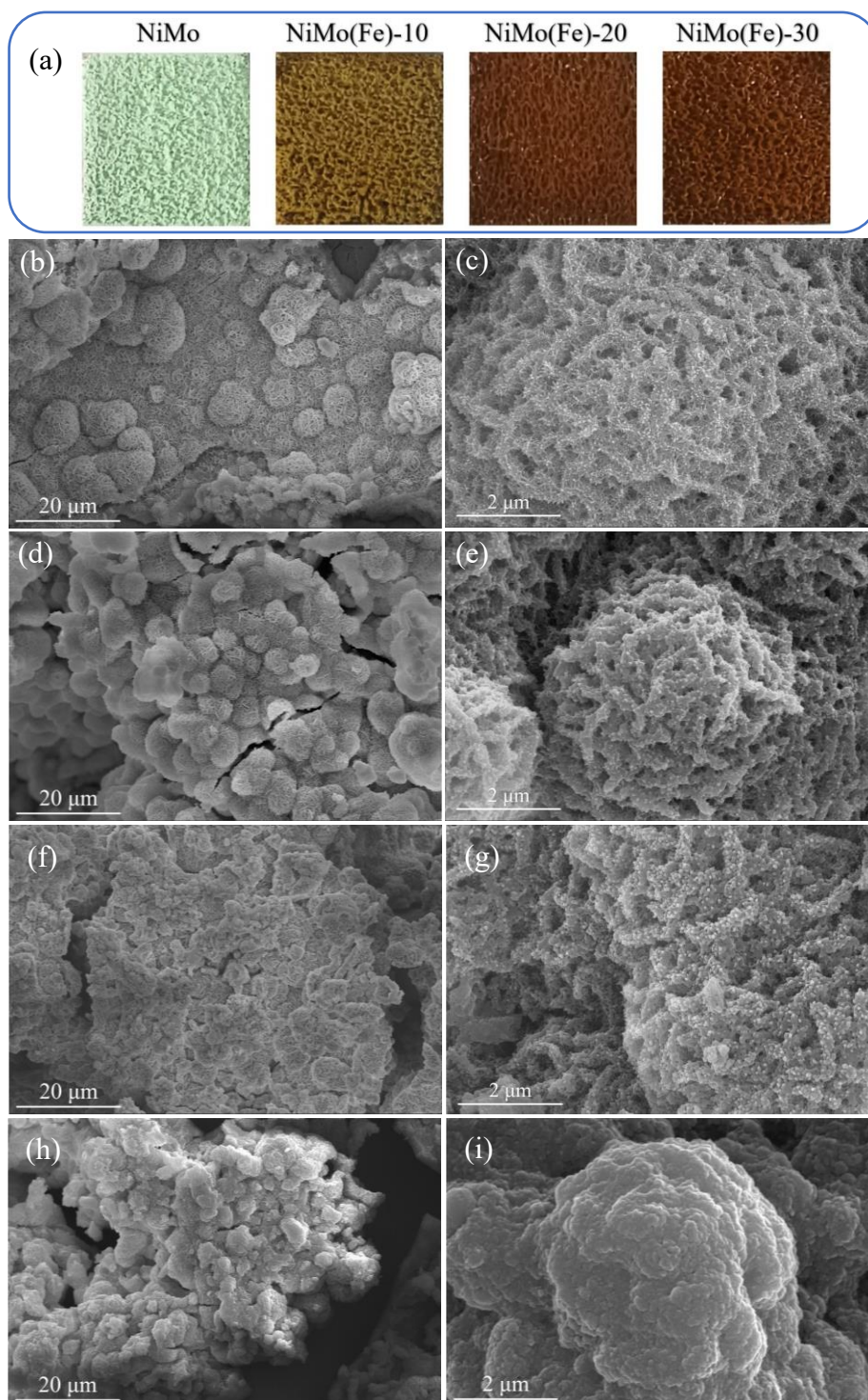


Figure S3. The photos of four NiMo-based samples (a). SEM images of NiMo (b,c), NiMo(Fe)-10 (d,e), NiMo(Fe)-20 (f,g), and NiMo(Fe)-30 (h,i) samples.

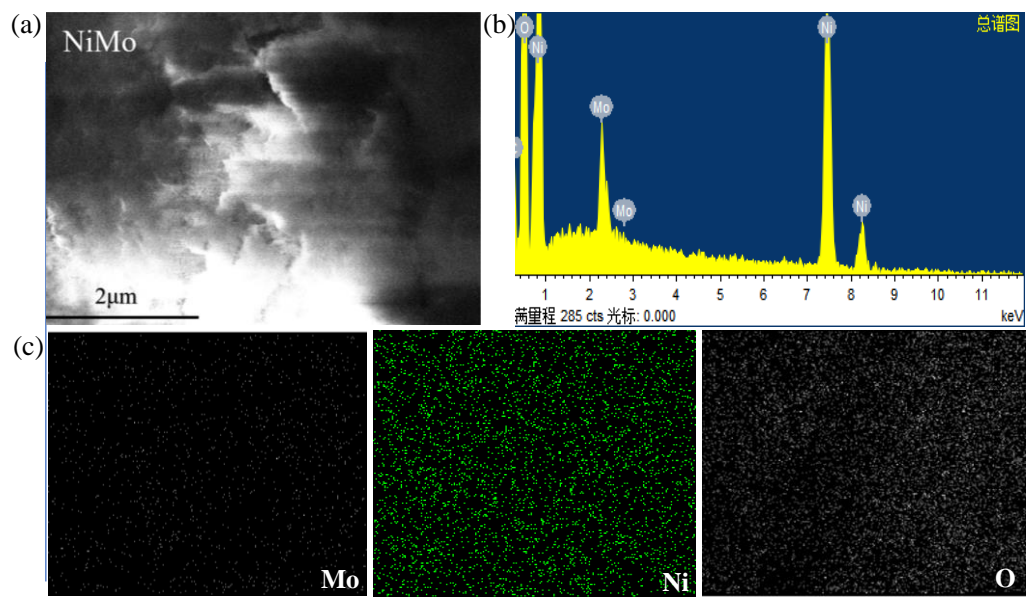


Figure S4. EDS of NiMo catalyst.

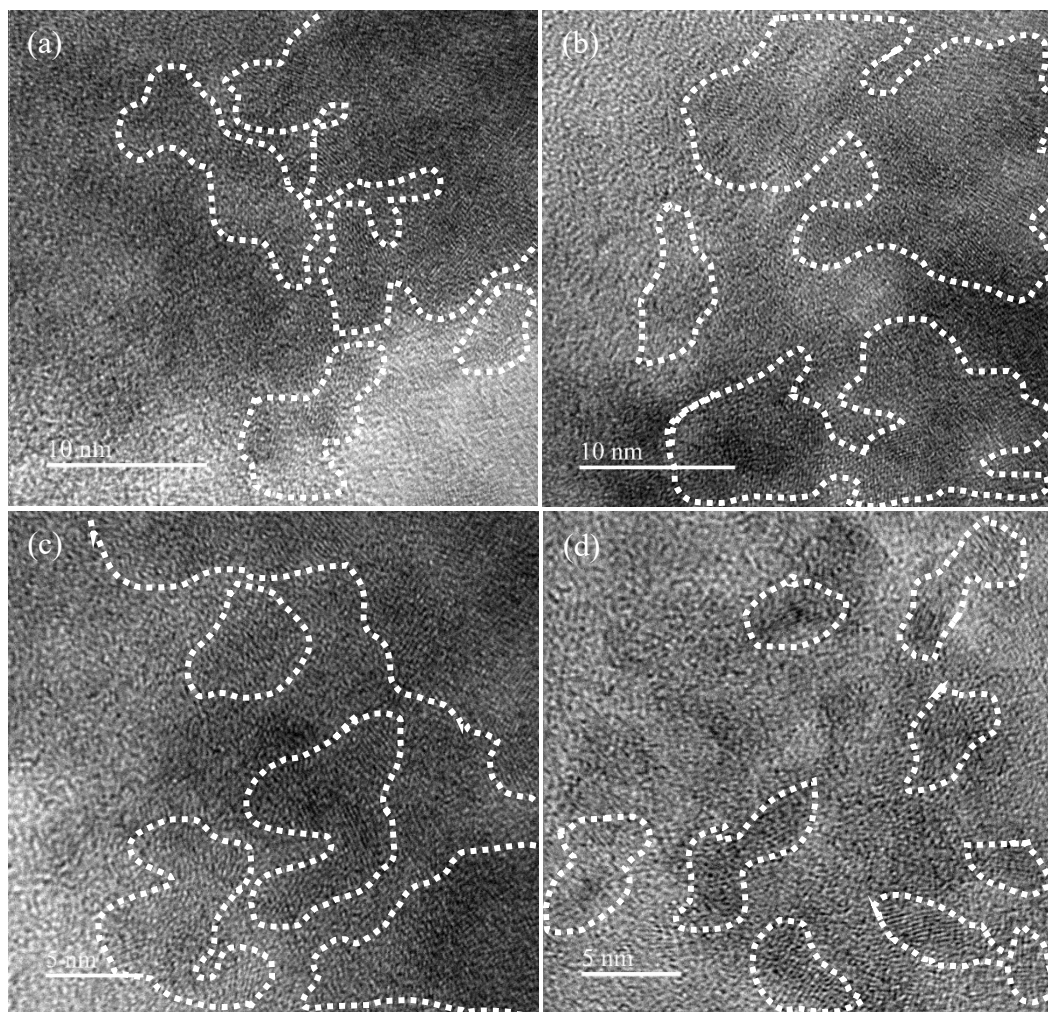


Figure S5. The HRTEM images of several NiMo(Fe)-20 samples.

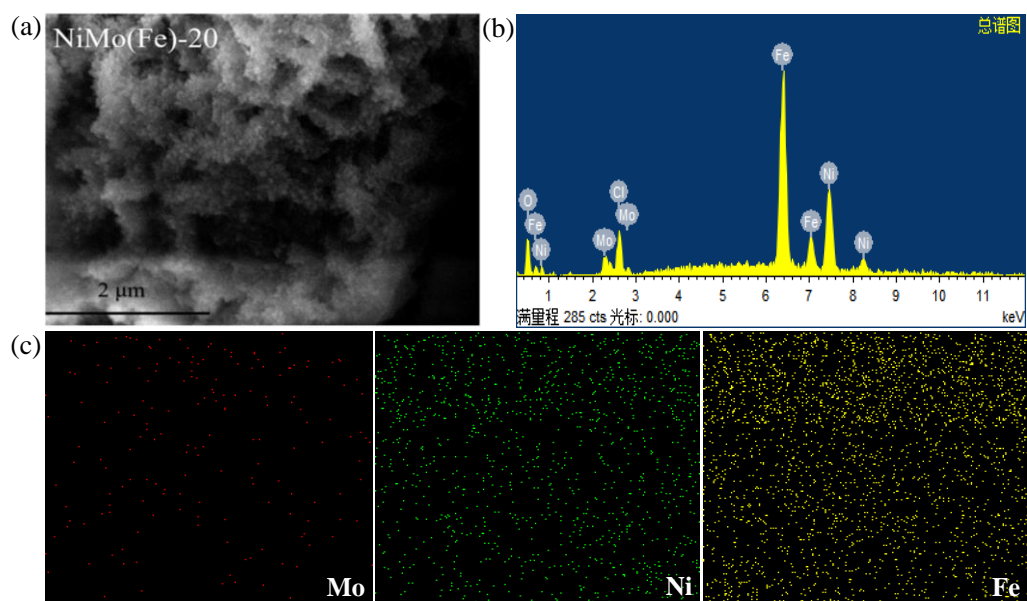


Figure S6. EDS of NiMo(Fe)-20 catalyst.

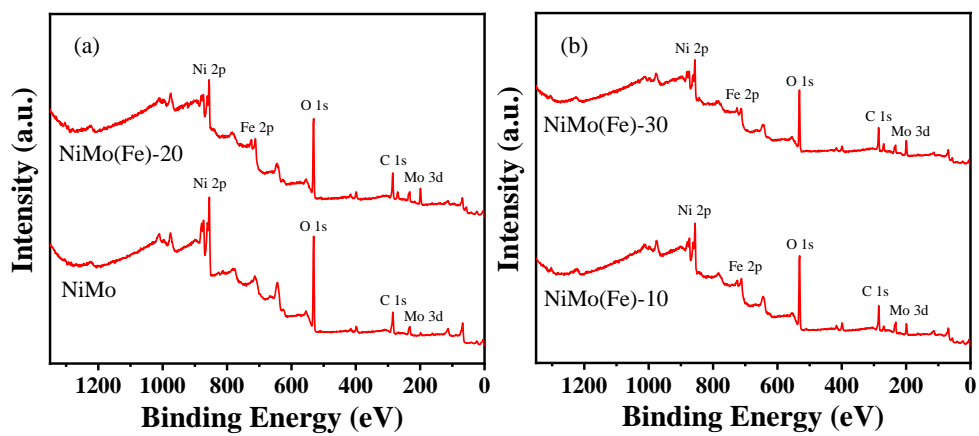


Figure S7. XPS survey spectra of NiMo, NiMo(Fe)-20, NiMo(Fe)-10, and NiMo(Fe)-30 samples.

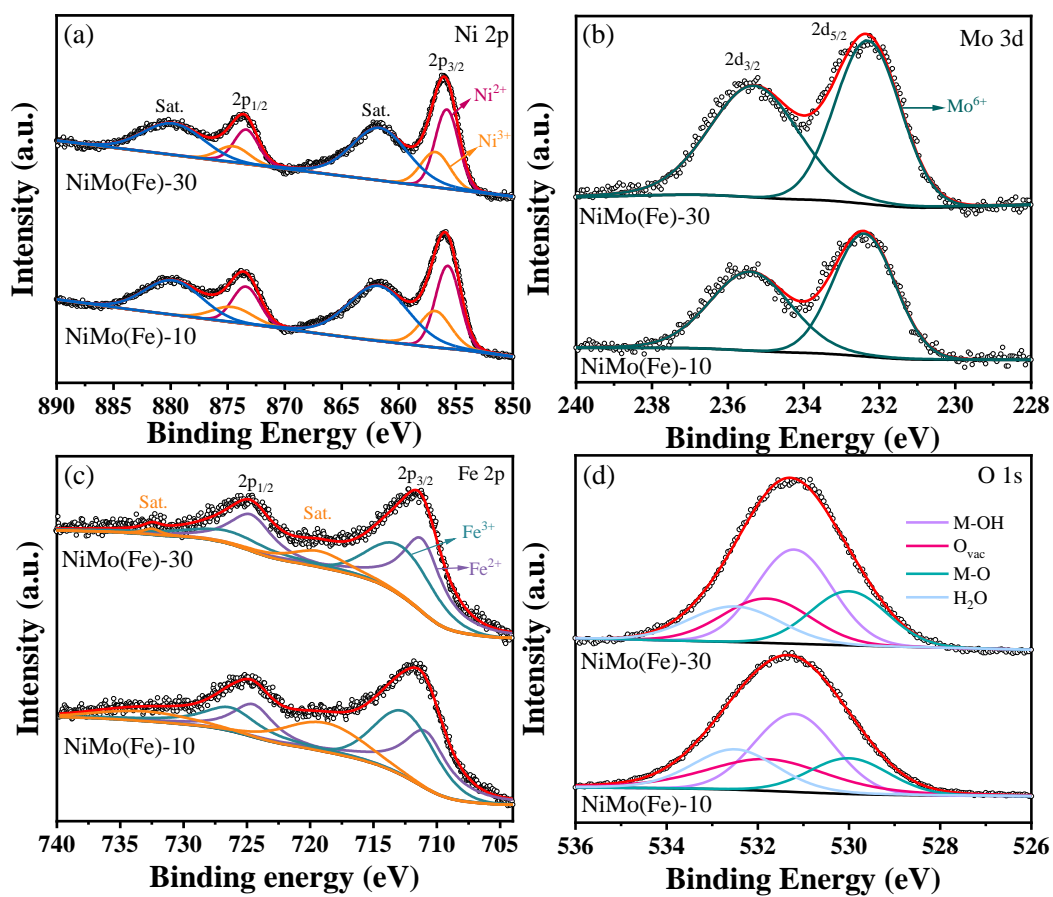


Figure S8. (a) Ni 2p, (b) Mo 3d, (c) Fe 2p, and (d) O 1s spectra of NiMo(Fe)-10 and NiMo(Fe)-30 sample.

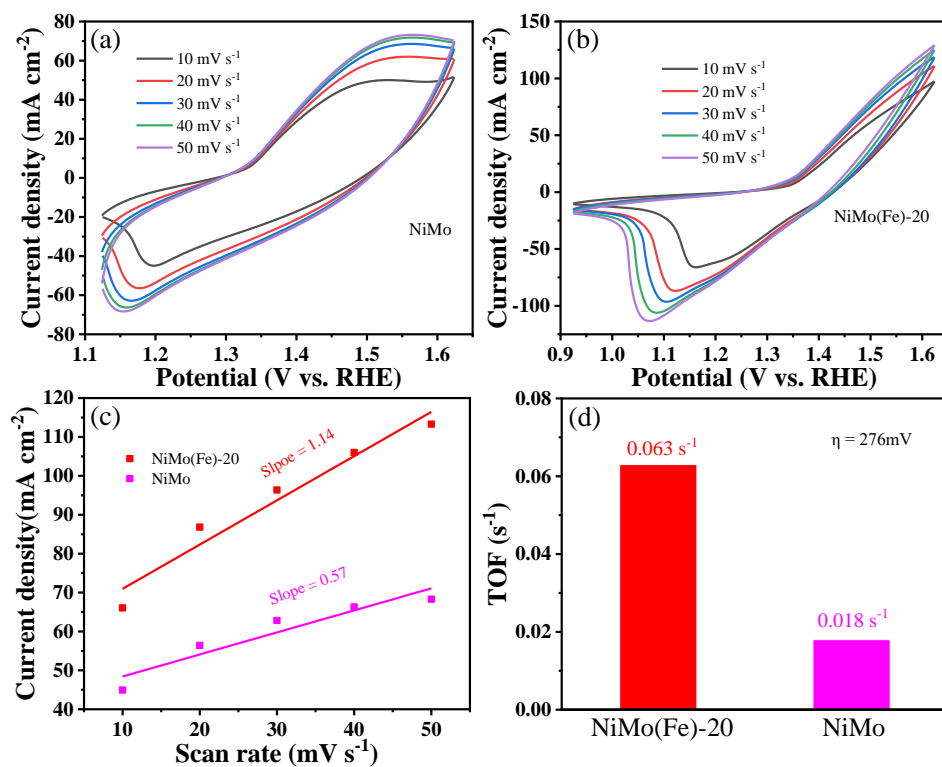


Figure S9. CV curves at different scan rates of NiMo and NiMo(Fe)-20 catalysts (a, b); Corresponding linear relationships of peak currents versus scan rates (c); TOF values (d).

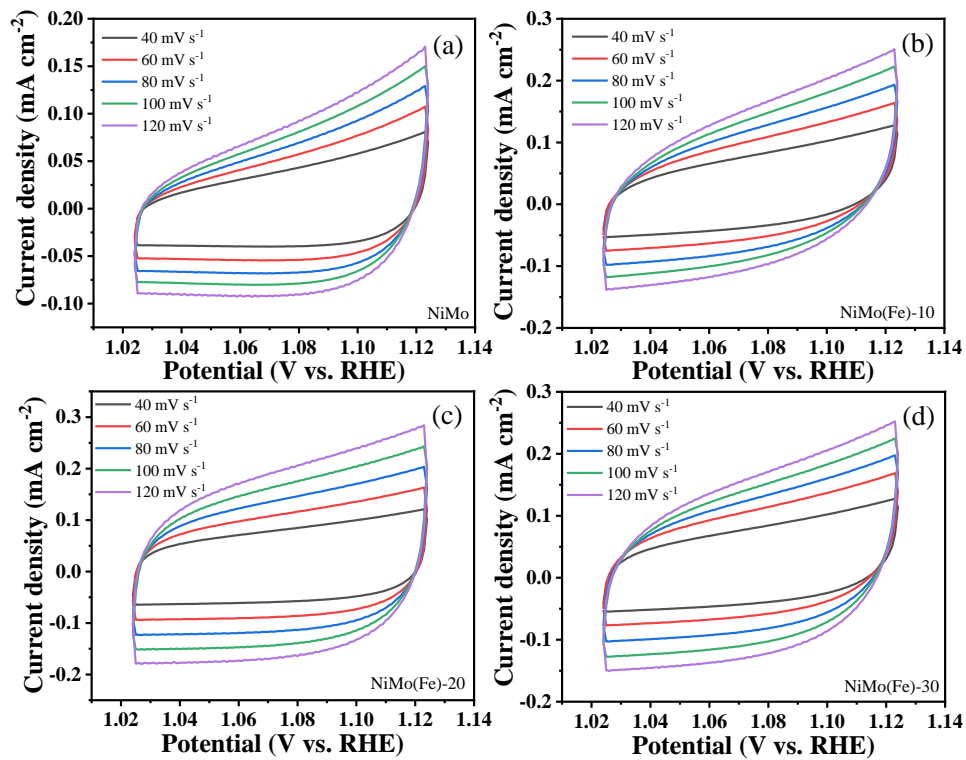


Figure S10. CV curves from 1.024 V to 1.124 V at the scan rates of 40, 60, 80, 100 and 120 mV s<sup>-1</sup>.

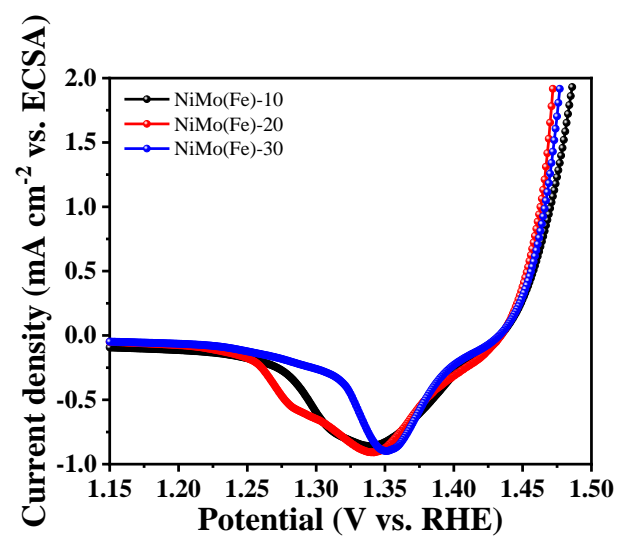


Figure S11. LSV curves normalized by ECSA.

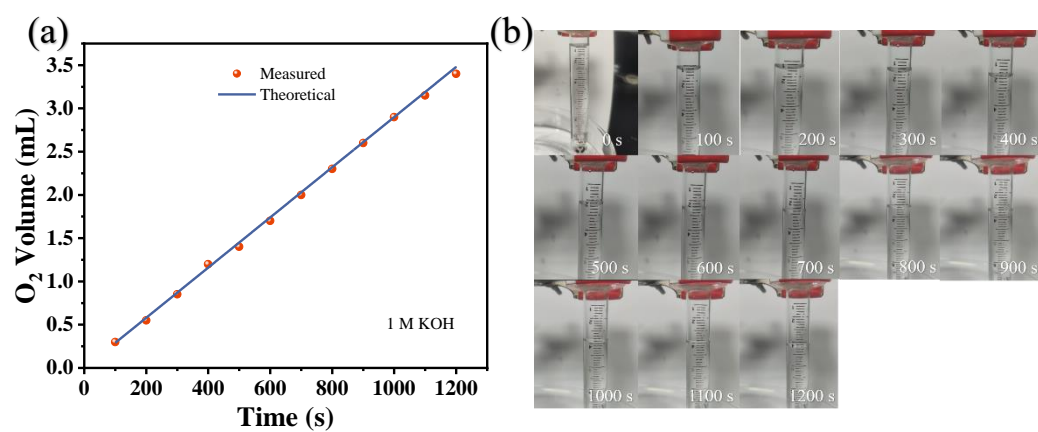


Figure S12. (a) Measured and calculated volume of O<sub>2</sub> for NiMo(Fe)-20. (b) Digital photographs of collected O<sub>2</sub> in 1.0 M KOH.

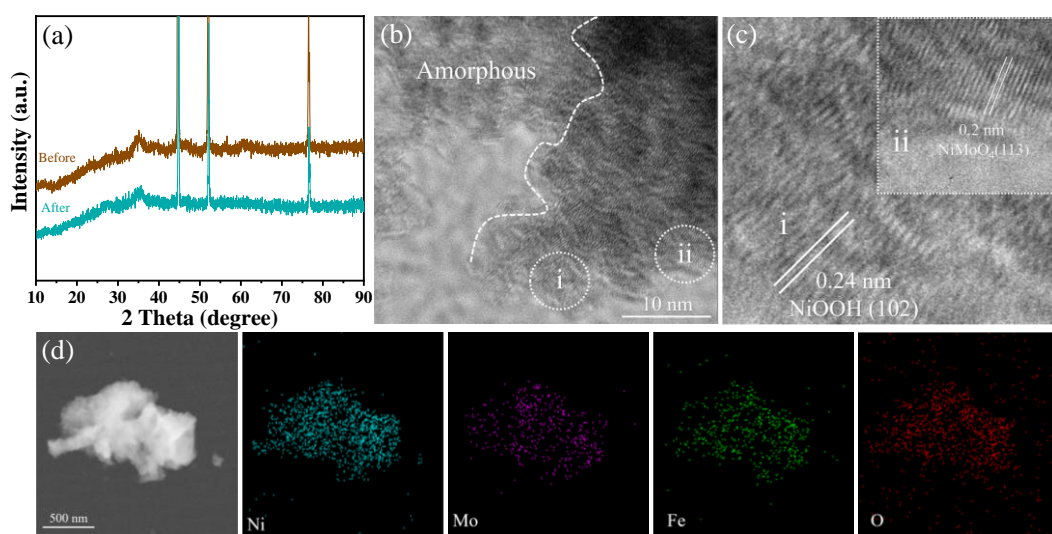


Figure S13. XRD patterns (a); TEM and HRTEM images (b, c); and element mappings (d) of NiMo(Fe)-20 after stability test.

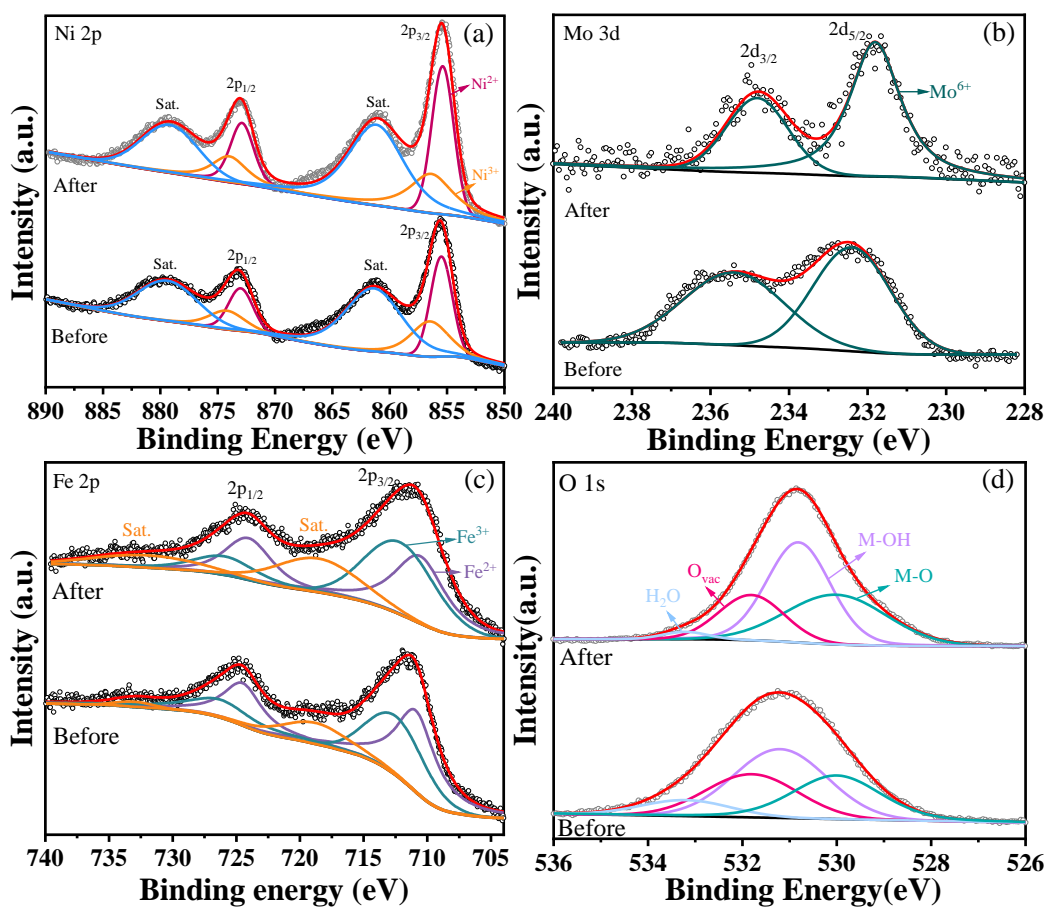


Figure S14. XPS spectra of (a) Ni 2p, (b) Fe 2p, (c) Mo 3d, and (d) O 1s of NiMo(Fe)-20 before and after stability test.

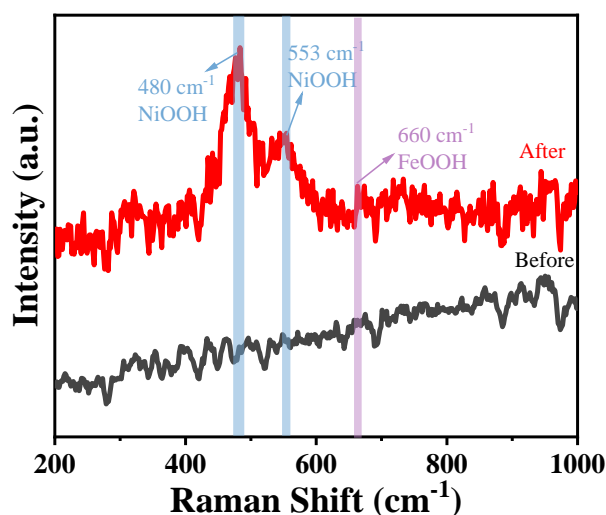


Figure S15. Raman spectra of NiMo(Fe)-20 before and after stability test.

We didn't find the lattice fringes of FeOOH species in HRTEM images. In addition, the percentage of Fe<sup>3+</sup> in the HRXPS of Fe 2p only changed from 36.4% to 36.7% after the stability test, implying that the Fe species hardly underwent surface reconstruction during the electrochemical test. Furthermore, the formation of NiOOH species was further verified by Raman spectra. In Figure S14, the two bands centered at ca. 480 and 553.6 cm<sup>-1</sup> are associated with NiOOH, and the additional band at ~660 cm<sup>-1</sup> confirms the formation of FeOOH. However, the Raman peak intensity of FeOOH is very weak, which means that only a small amount of Fe is oxidized during the electrochemical process, which is consistent with the XPS results. Therefore, Fe<sup>3+</sup> can promote the generation of high-valent nickel species, and the active nickel species are considered as the main active sites to enhance OER activity.

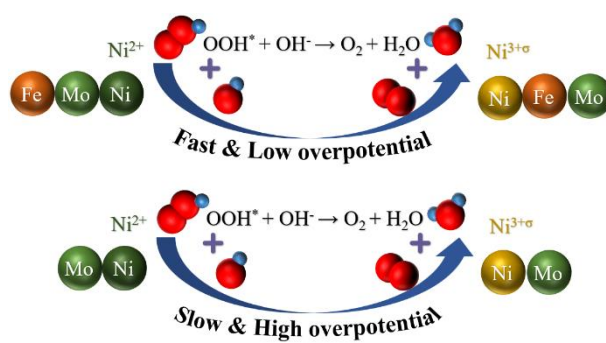


Figure S16. The possible reaction mechanism of NiMo(Fe)-20 and NiMo catalysts.

Table S1. Comparison of OER performance in alkaline media.

Catalysts	Electrolyte	j (mA cm <sup>-2</sup> )	$\eta$ /mV	Ref.
NiMo(Fe)-20	1 M KOH	100	239	This work
NiSe <sub>2</sub> -NiMoO <sub>4</sub> /NF	1 M KOH	100	330	1
Ni <sub>x</sub> S <sub>y</sub> @MnO <sub>x</sub> H <sub>y</sub> /NF	1 M KOH	100	326	2
Fe-Ni <sub>2</sub> P/MoS <sub>x</sub> /NF	1 M KOH	100	326	3
NiCr-LDH NSAS	1 M KOH	100	280	4
NiIr-LDH	1 M KOH	100	279	5
Cu-Ni <sub>3</sub> S <sub>2</sub> @NiFe LDH-200	1 M KOH	100	310	6
Au@Ni(Fe)OOH	1 M KOH	100	290	7
CoNiN@NiFe-LDH	1 M KOH	100	291	8
Ni <sub>2</sub> P-Co <sub>2</sub> P-0.5	1 M KOH	100	340	9
NiSe@CoFe LDH/NF	1 M KOH	100	236	10

Table S2. Comparison of electrochemical water splitting performance in 1 M KOH electrolyte.

Electrolyzer	Cell Voltages (V)		Ref.
	E-10	E-100	
Pt/C  NiMo(Fe)-20	1.44	1.53	This work
Cu-Ni <sub>3</sub> S <sub>2</sub> @NiFe LDH-200  Cu-Ni <sub>3</sub> S <sub>2</sub> @NiFe LDH-100	1.502	~	6
CoNiN@NiFe-LDH  CoNiN	1.58	1.76	8
Ni <sub>2</sub> P-Co <sub>2</sub> P-0.5  Ni <sub>2</sub> P-Co <sub>2</sub> P-1	1.6	~	9
NiSe@CoFe LDH  Pt/C	~	1.56	10
Mo-Ni <sub>2</sub> P@NiFe LDH/NF  Mo-Ni <sub>2</sub> P@NiFe LDH/NF	1.46	~	11
NiCo LDH@NiCoP/NF  NiCo LDH@NiCoP/NF	1.54	~	12
Mo-Ni <sub>3</sub> S <sub>2</sub> @NiFe  Mo-Ni <sub>3</sub> S <sub>2</sub> @NiFe	1.54	~	13
P-Ni <sub>0.75</sub> Fe <sub>0.25</sub> Se <sub>2</sub>   MoNi <sub>4</sub> /MoO <sub>2</sub>	~	1.61	14
Gd-NiFe-LDH/CC  Pt/C/CC	1.46	1.55	15
NiFeMo  NiFeMo	1.59	1.8	16
NiCoP NR@NS  NiCoP NR@NS	1.57	1.74	17
MH-TMO	1.49	1.67	18
P-Ni <sub>3</sub> S <sub>2</sub> /CoFe <sub>2</sub> O <sub>4</sub> /NF  Pt/C/NF	1.486	1.577	19

## References

- 1 T. Yu, Q. Xu, J. Chen, G. Qian, X. Zhuo, H. Yang and S. Yin, *Chem. Eng. J.*, 2022, **449**, 137791–137800.
- 2 P. Wang, Y. Luo, G. Zhang, Z. Chen, H. Ranganathan, S. Sun and Z. Shi, *Nano-Micro Lett.*, 2022, **14**, 120–136.
- 3 X. Zhang, C. Liang, X. Qu, Y. Ren, J. Yin, W. Wang, M. Yang, W. Huang and X. Dong, *Adv. Mater. Inter.*, 2020, **7**, 1901926–1901932.
- 4 X. Zhang, X. Sun, Y. Li, F. Hu, Y. Xu, J. Tian, H. Zhang, Q. Liu, H. Su and S. Wei, *J. Mater. Chem. A*, 2021, **9**, 16706–16712.
- 5 H. You, D. Wu, D. Si, M. Cao, F. Sun, H. Zhang, H. Wang, T.-F. Liu and R. Cao, *J. Am. Chem. Soc.*, 2022, **144**, 9254–9263.
- 6 Y. Ding, X. Du and X. Zhang, *Appl. Surf. Sci.*, 2022, **584**, 152622–152634.
- 7 X. Liu, S. Jing, C. Ban, K. Wang, Y. Feng, C. Wang, J. Ding, B. Zhang, K. Zhou, L. Gan and X. Zhou, *Nano Energy*, 2022, **98**, 107328–107338.
- 8 J. Wang, G. Lv and C. Wang, *Appl. Surf. Sci.*, 2021, **570**, 151182–151191.
- 9 C. Zhang, X. Du and X. Zhang, *Int. J. Hydrog. Energy*, 2022, **47**, 14515–14527.
- 10 F. Nie, Z. Li, X. Dai, X. Yin, Y. Gan, Z. Yang, B. Wu, Z. Ren, Y. Cao and W. Song, *Chem. Eng. J.*, 2022, **431**, 134080–134090.
- 11 Z. Yang, Y. Lin, F. Jiao, J. Li, J. Wang and Y. Gong, *J. Energy Chem.*, 2020, **49**, 189–197.
- 12 L. Zhang, J. Peng, Y. Yuan, W. Zhang and K. Peng, *Appl. Surf. Sci.*, 2021, **557**, 149831–149840.
- 13 X. Feng, Y. Shi, J. Shi, L. Hao and Z. Hu, *Int. J. Hydrog. Energy*, 2021, **46**, 5169–5180.
- 14 Y. Huang, L.-W. Jiang, X.-L. Liu, T. Tan, H. Liu and J.-J. Wang, *Appl. Catal. B-Environ.*, 2021, **299**, 120678–120687.
- 15 M. Li, H. Li, X. Jiang, M. Jiang, X. Zhan, G. Fu, J.-M. Lee and Y. Tang, *J. Mater. Chem. A*, 2021, **9**, 2999–3006.
- 16 Z. Lv, Z. Li, X. Tan, Z. Li, R. Wang, M. Wen, X. Liu, G. Wang, G. Xie and L. Jiang, *Appl. Surf. Sci.*, 2021, **552**, 149514–149522.
- 17 J.-G. Wang, W. Hua, M. Li, H. Liu, M. Shao and B. Wei, *ACS Appl. Mater. Inter.*, 2018, **10**, 41237–41245.

18 F. Hu, D. Yu, M. Ye, H. Wang, Y. Hao, L. Wang, L. Li, X. Han and S. Peng, *Adv. Energy Mater.*, 2022, **12**, 2200067–2200076.

19 J.-J. Duan, R.-L. Zhang, J.-J. Feng, L. Zhang, Q.-L. Zhang and A.-J. Wang, *J. Colloid Interface Sci.*, 2021, **581**, 774–782.